Atomic Force Microscopy and Analytical Ultracentrifugation for Probing Nanomaterial Protein Interactions

Jens Schaefer,[†,∥] Christine Schulze,[‡,∥] Elena Eva Julianne Marxer,[†] Ulrich Friedrich Schaefer,[‡] Wendel Wohlleben,[§] Udo Bakowsky,[†] and Claus-Michael Lehr[‡,⊥,*]

[†]Department of Pharmaceutics and Biopharmacy, Philipps-University Marburg, Marburg, Germany, [‡]Biopharmaceutics and Pharmaceutical Technology, Saarland University, Saarbruecken, Germany, [§]Polymer Physics Research, BASF SE, Ludwigshafen, Germany, and [⊥]Helmholtz Institute for Pharmaceutical Research, Saarbruecken, Germany. [∥]These authors contributed equally to this work.

ABSTRACT Upon contact with the human body, nanomaterials are known to interact with the physiological surroundings, especially with proteins. In this context, we explored analytical methods to provide biologically relevant information, in particular for manufactured nanomaterials as produced by the chemical industry. For this purpose, we selected two batches of SiO_2 nanoparticles as well as four batches of CeO_2 nanoparticles, each of comparably high chemical purity and similar physicochemical properties. Adsorption of serum proteins and bovine serum albumin (BSA) was quantified by SDS-PAGE in combination with densitometry and further investigated by atomic force microscopy (AFM) and analytical ultracentrifugation (AUC). The protein adsorption to SiO_2 nanoparticles was below the limit of detection, regardless of adjusting pH or osmolality to physiological conditions. In contrast, the four CeO_2 nanomaterials could be classified in two groups according to half-maximal protein adsorption. Measuring the work of adhesion and indention by AFM for the BSA-binding CeO_2 nanomaterials revealed the same classification, pointing to alterations in shape of the adsorbed protein. The same trend was also reflected in the agglomeration behavior/dispersibility of the four CeO_2 nanomaterials as revealed by AUC. We conclude that even small differences in physicochemical particle properties may nevertheless lead to differences in protein adsorption, possibly implicating a different disposition and other biological responses in the human body. Advanced analytical methods such as AFM and AUC may provide valuable additional information in this context.

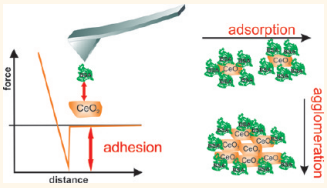

KEYWORDS: SiO_2 nanoparticles · CeO_2 nanoparticles · bovine serum albumin · work of adhesion · surface free energy · SDS-PAGE · agglomeration · force distance curves

Engineered nanomaterials with novel properties are one of the century's key technologies, offering extraordinary opportunities for various technical applications such as electronics, energy management, construction, and information technology, but also in pharmacy and medicine. Because the miniaturization of materials into the nanosize range may dramatically change physical and chemical properties, nanomaterials will obviously also interact in a different way with biological systems. In particular the adsorption of proteins is considered as a key issue regarding the safety of nanomaterials for environment and health.[1,2]

While after inhalation or ingestion only a relatively small fraction (1% or less) may translocate into the bloodstream,[3] there is a risk of agglomeration due to the biopersistence of most engineered nanomaterials. The biodistribution of nanomaterials is likely to strongly depend on adsorption of proteins occurring in the various body compartments and liquids. Xia *et al.* developed a model for the adsorption of small molecules to nanoparticles, when specific characteristics of the particle and adsorbent are given.[4] The Dawson group has pioneered structure–property relationships in protein coronas during the past few years,[5−9] and the biophysics of adsorbed proteins has been reviewed recently.[10] The majority of the few studies on metal oxides found adsorption of albumin (in serum) or humic acid (in soil), ensuing increased dispersibility.[10,11] Cedervall *et al.* investigated the complete protein corona of serum albumin and quantified human serum albumin and fibrinogen on polymeric nanoparticles using methods such as microcalorimetry and surface plasmon resonance.[12] Recently, Rocker *et al.* studied the adsorption of albumin in greater detail, including on/off rates, adsorption affinity, and monolayer saturation on polymer-coated FePt and CdSe/ZnS nanoparticles, using fluorescence correlation spectroscopy.[13]

The application of standard methods for measuring protein adsorption phenomena such as microcalorimetry, surface plasmon resonance, or ultrasound resonator technology was found to be difficult for metal oxide particles, as we observed rapid sedimentation

* Address correspondence to lehr@mx.uni-saarland.de.

Received for review November 9, 2010 and accepted May 11, 2012.

Published online May 11, 2012
10.1021/nn202657q

and were facing irreversible contamination of the equipment. Fluorescence correlation spectroscopy would require fluorescence properties of the particles, which is usually not the case for such materials. Thus, it appears that all these methods are not easily transferable to industrially relevant nanomaterials. Instead, we decided to explore biochemical methods such as SDS-PAGE, Coomassie staining, and densitometry in combination with atomic force microscopy (AFM) and analytical ultracentrifugation (AUC).

Recently, Tenzer and colleagues performed a proteomic approach on amorphous silica nanoparticles after incubation in serum, finding quantitative differences of the protein corona depending on the particle size.[14] Monopoli and co-workers compared the hard corona of sulfonated polystyrene particles to that of silica particles and found that the protein concentration can significantly influence the protein decoration.[8] Still, those studies were performed with well-defined model particles. For our work we chose two batches of SiO_2 nanoparticles (Levasil 50 and 200, AkzoNobel Chemcals GmbH, Düren, Germany), which are sold as a bulk product for the stabilization of paints and lacquers and as an additive in plaster and concrete.

As a second industrially relevant nanomaterial we chose four batches of CeO_2 nanoparticles, which are marketed as oxidative catalysts for self-cleaning surfaces in ovens,[15] as catalytic diesel fuel additives,[16] and as an abrasive for chemical-mechanical polishing in electronic chip wafer production. The effect of CeO_2 particles from, for example, diesel fuel or from abrasion of coatings exposed to the environment was recently analyzed by van Hoecke *et al.*[2] They investigated three different sizes (14, 20, and 29 nm) of CeO_2 particles in different aquatic toxicity tests. The differences in toxicity could not be explained by a direct effect of dissolved Ce ions or CeO_2 NP uptake or by physical effects such as light restriction. Additionally they found that the particle properties—especially the higher surface area of smaller particles—have an influence on the toxicity of CeO_2 NPs. Substrates for these investigations were three batches of cerium dioxide nanoparticles (CeO_2 A–C), each prepared industrially by flame pyrolysis.[17] An additional batch of highly pure nanoparticle (CeO_2 D), prepared by wet precipitation, was included as reference material.[18]

RESULTS

Physicochemical Characterization of Particles. Intrinsic properties of the materials are essential to interpret the protein adsorption patterns in protein-containing suspension. Such intrinsic physicochemical properties of the investigated particles are summarized in Table 1 and Figures 1 and 2.

The two SiO_2 nanoparticles are amorphous and uniformly round in shape (see Figure 1). The nomenclature of Levasil 50 and 200 is derived from the BET

TABLE 1. Physicochemical Characterization of the Tested Nanoparticles

method	CeO_2 A	CeO_2 B	CeO_2 C	CeO_2 D	SiO_2 50	SiO_2 200
XRD purity and crystalline phase	>99.9% purity, cerianite, cubic	>99.9% purity, cerianite, cubic	>99% purity, cerianite, cubic	>99% purity, cerianite + amorphous	>99% amorphous	>99% amorphous
XPS surface chemistry [at%]	O 57 | Ce 25 | C 18	O 56 | Ce 22 | C 22	O 53 | Ce 26 | C 20 | Cl 0.6	O 57 | Ce 27 | C 15 | N 0.8	O 53 | Si 40 | C 5| Na 2 | N 0.3 | Cl 0.5	O 65 | Si 29 | C 4 | Na 1| N 0.6
SIMS surface organic contaminations	CeO_2 cluster, Na, organics	CeO_2 cluster, Na, organics	CeO_2 cluster, Na, organics, Li	CeO_2 cluster, ×2 less organics than CeO_2 A–C, Na	SiO_2 cluster, less organics than SiO_2 200	SiO_2 cluster, Na, Cl, organics, traces of surfactant
BET surface [m^2/g]	63[a]	44[a]	33[a]	n.d.	50[f]	200[f]
surface energy [mN/m] (disperse + polar parts)[b]	72.5 (41.4 + 31.1)	71.0 (42.3 + 28.7)	69.1 (40.6 + 28.5)	>73.5 (42.2 + 31.2)	n.d.	n.d.
specific polar interaction with acetonitrile [kJ/mol][c]	n.d.	17.5	20.2	n.d.	28.4	30.5
pH[d]	5.9	6.2	5.9	5.5	8.9	9.5
TEM diameter ± SD [nm]	11.6 ± 5.6	22.6 ± 5.7	22.5 ± 7.6	5.4 ± 1.3	91.0 ± 19.5	27.1 ± 5.9
DLS diameter ± SD [nm] (PDI)[d,e]	180.8 ± 3.0 (0.257)	189.2 ± 1.4 (0.225)	170.4 ± 2.1 (0.170)	163.4 ± 23.5 (0.311)	114.4 ± 1.0 (0.071)	35.6 ± 1.2 (0.19)
Zeta-potential ± SD [mV][d,e]	40.9 ± 1.7	38.3 ± 4.8	31.5 ± 3.5	28.8 ± 1.4	−39.0 ± 0.4	−32.7 ± 1.2

[a] BET surface according to NanoCare Final Scientific Report.[16] [b] Determined with contact angle measurement. [c] Own measurements with inverse gas chromatography at 1% surface coverage. [d] 10 mg/mL of nanoparticle dispersed in deionized water for measurement. [e] Particle size and zeta potential in dispersion were measured with a ZetaSizer Nano (Malvern). [f] According to manufacturer. n.d. means not determined.

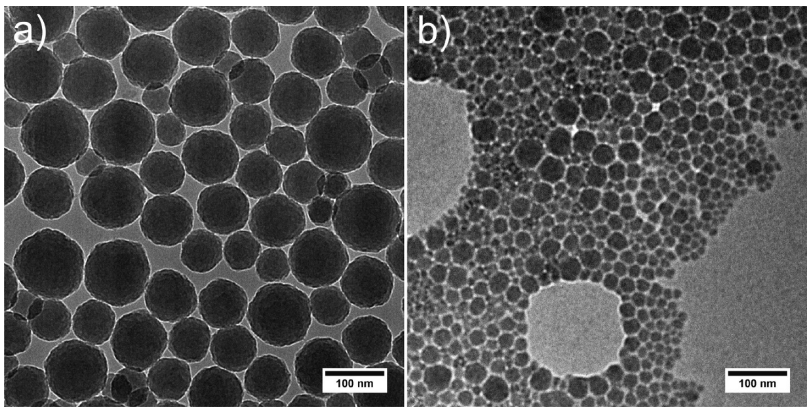

Figure 1. TEM images of (a) SiO_2 50; (b) SiO_2 200 (50.000× magnification (300.000 V)).

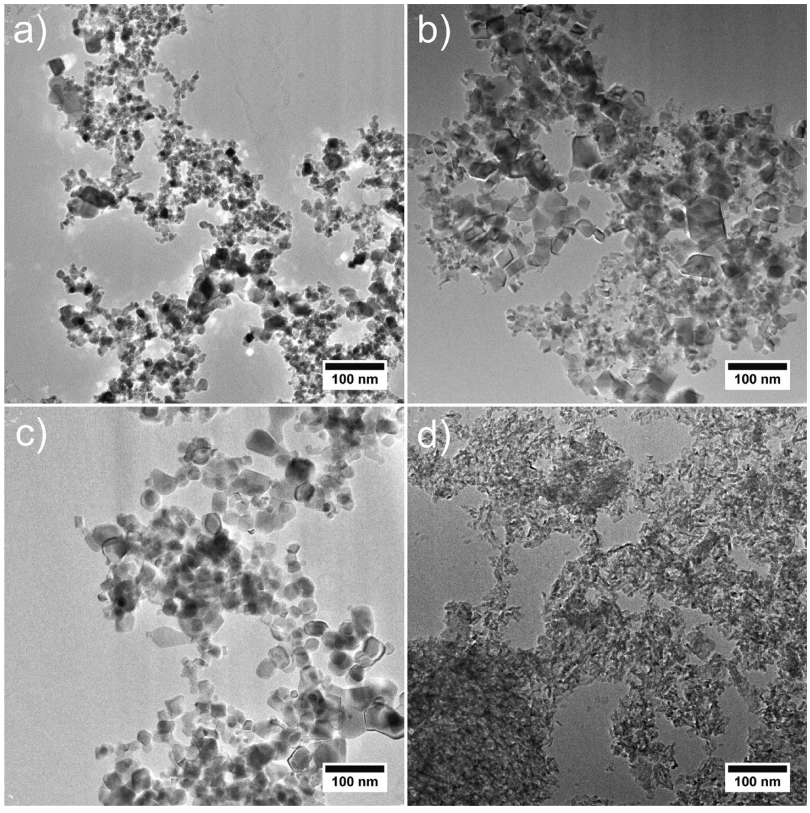

Figure 2. TEM images of (a) CeO_2 A particles; (b) CeO_2 B particles; (c) CeO_2 C particles; (d) CeO_2 D particles (50.000× magnification (300.000 V)).

surface of these two nanomaterials, the mean TEM diameter being approximately 91 and 27 nm, respectively, and both batches were received as aqueous dispersions of single particles without agglomeration. The surface of the particles is very clean; only marginal organic impurities can be found on the surface (from secondary ion mass spectrometry (SIMS)). A clean surface and well-defined particle shape and size distributions would facilitate the interpretation of protein adsorption data. Since adsorption processes should be governed by surface energy and polarity, we performed inverse gas chromatography, which reveals a highly polar surface, as the specific surface interaction with the polar solvent acetonitrile was very high (see Table 1). Determination of the contact angles was not possible due to these extremely polar surfaces, such that the particles could not be fixed on any suitable substrate (data not shown). The zeta potential with −58 mV for SiO_2 50 and −49 mV for SiO_2 200 is highly negative, and the pH of the aqueous dispersion with values of 8.9−9.5 is slightly alkaline.

The formulations of CeO_2 A to D tend to form aggregates, as can be seen in Figure 2. TEM images show square-cut crystalline particles for all CeO_2 A to C, but CeO_2 D reveals a more amorphous structure and smaller primary particle sizes (TEM diameter, see

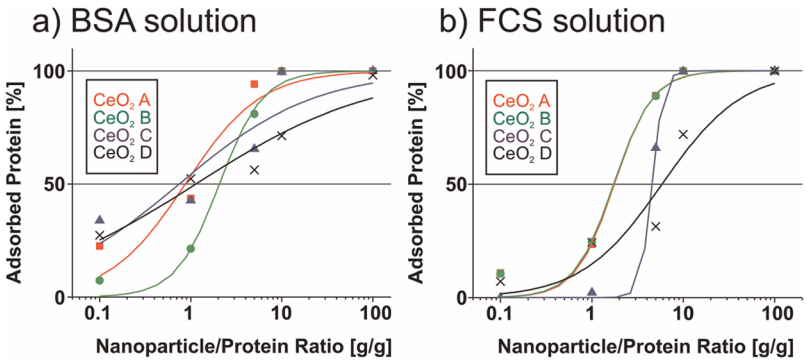

Figure 3. Adsorption isotherms for CeO_2 A–D (squares: CeO_2 A, circles: CeO_2 B, triangles: CeO_2 C, ×'s: CeO_2 D), determined with densitometry for (a) BSA or (b) total FCS protein. CeO_2 A and B reveal similar adsorption patterns (especially for FCS), while CeO_2 C shows an adsorption pattern more similar to CeO_2 D (especially for BSA).

Table 1). The particle surfaces were indistinguishable within the error margins, except that CeO_2 C showed additional Cl and Li (from X-ray photoelectron spectroscopy (XPS) and SIMS) and that the CeO_2 D particle surface is much less contaminated with organic material than the other three particles.

For CeO_2 A to D, we compared contact angles of a thin planarized powder film with drops of water, formamide, and diiodomethane. The drops were imaged onto a charge-coupled device (CCD), and contact angles were extracted by standardized software. After Owens–Wendt evaluation, all samples are hydrophilic, with total surface energies of 72.5, 71.0, 69.1, and >73.5 mN/m for CeO_2 A, B, C, and D, respectively. The dispersed part of the surface energy (related to unspecific van der Waals interactions) is lowest for CeO_2 C, with 40.6 mN/m, *versus* 41.1, 42.3, and 42.2 mN/m for CeO_2 A, B, and D.

The sizes of the different CeO_2 particles measured with dynamic light scattering (DLS) are practically uniform, ranging from 163.4 nm for CeO_2 D to 189.2 nm for CeO_2 B. The zeta potentials of all particles are positive in the range 29 to 41 mV and comparable to the manufacturer's reference data (data not shown). The pH of the particle dispersions in double-distilled water varied between 5.5 and 6.2.

Quantification of Protein Adsorption. The amount of particle-bound protein was calculated from the protein fraction remaining in the supernatant after incubation and removal of particles and adsorbed corona by centrifugation. The nonadsorbed protein fraction in the supernatant was quantified (a) densitometrically after SDS-PAGE and Coomassie staining and (b) by mass-selective detection of bovine serum albumin (BSA) (AUC).

a. SDS-PAGE. Dispersion of SiO_2 50 and SiO_2 200 in BSA solution did not lead to any detectable protein adsorption. Also, no BSA adsorption occurred after incubation of SiO_2 50 and SiO_2 200 in FCS (fetal calf serum). (For details, see Supporting Information, Figures S1–S3.) Neither an adjustment to a pH of 6 nor dispersion of the particles in physiological phosphate buffered saline (PBS) increased the BSA adsorption to detectable amounts. Thus there were no data that would have allowed calculating protein binding behavior from adsorption isotherms for the SiO_2 nanoparticles.

In contrast, significant protein adsorption was measured for the CeO_2 particles. Plotting the amount of adsorbed protein from densitometry data of supernatants against the nanoparticle–protein ratio led to a sigmoid pattern for all CeO_2 particles tested (see Figure 3). As it appears, two classes of similar protein adsorption behavior can be distinguished for the four particles: For both BSA and FCS, CeO_2 A and B show very similar if not identical adsorption isotherms. *Vice versa*, the isothermes of CeO_2 C and D are relatively similar to each other as well, clearly different from those of CeO_2 A and B. The strikingly similar protein adsorption behavior of CeO_2 A and B is also reflected very well by the half-maximum adsorption values and Hill slopes for both proteins, respectively. In the case of CeO_2 C and D at least one of the two parameters (Hill slope for BSA, half-max adsorption for FCS) shows similar values (see Table 2).

b. Mass Selective Detection of BSA by Analytical Ultracentrifugation. AUC measurements were performed with FCS solution, but only the mass-selected fractions of 60–80 kDa and 100–140 kDa (assumed to represent BSA) were quantified and fitted to a sigmoidal model. This method confirmed the results obtained with SDS-PAGE: The BSA signal in the presence of SiO_2 50 and 200 was not reduced compared to the control experiment without particles, also supporting that BSA was obviously not adsorbed. In contrast, a clear reduction of the BSA peak could be seen in the presence of the tested CeO_2 particles. For CeO_2 A and CeO_2 B, the Hill slopes from FCS solution (by AUC; data not shown) agree excellently with the adsorbed BSA from FCS solution (determined by densitometry). Significantly fewer nanoparticles are required to deplete BSA from BSA solution than for FCS, since the adsorption isotherm is shifted to roughly 60% lower nanoparticle/protein values. Comparing half-maximal adsorption from BSA to that from FCS solution, a similar trend is seen.

TABLE 2. Summary of the Results Obtained with Atomic Force Spectroscopy, Densitometry after SDS-PAGE, and Analytical Ultracentrifugation for CeO_2 A to D

		CeO_2 A	CeO_2 B	CeO_2 C	CeO_2 D
AFM measurements	change of indention after BSA modification[a]	−10%	−12%	+10%	+26%
	change of force of adhesion after BSA modification[a]	+24%	+12%	−21%	−37%
	work of adhesion [mJ m^{-2}][a]	187 (+36)	172 (+18)	140 (−37)	158 (−95)
	surface free energy [mJ m^{-2}][a]	209 (+73)	176 (+35)	117 (−69)	149 (−232)
densitometry after SDS-PAGE	half-max adsorption of BSA ± SD [g/g][b]	0.86 ± 0.33	2.06 ± 0.26	0.74 ± 0.52	1.14 ± 0.51
	hill slope p for BSA adsorption[b]	1.06 ± 0.37	1.82 ± 0.27	0.58 ± 0.23	0.45 ± 0.1
	half-max adsorption of FCS ± SD [g/g][b]	1.76 ± 0.27	1.73 ± 0.26	4.55 ± 0.29	5.85 ± 1.96
	hill slope p for FCS adsorption[b]	2.07 ± 0.44	2.02 ± 0.42	7.12 ± 4.92	1 ± 0.4
AUC (BSA quantification)	half-max adsorption of BSA from FCS (AUC) ± SD [g/g]	6.3 ± 0.4	10 ± 3.8	2.5 ± 0.8	n.d.[e]
	hill slope p for BSA adsorption from FCS[c]	2.23 ± 0.27	1.98 ± 0.93	1.58 ± 0.82	n.d.
AUC (size distribution)	dispersibility (fraction <1 μm) [wt %][d]	24 ± 3	26 ± 3	9 ± 2	8 ± 2

[a] Atomic force measurements: change in the adhesion forces and indention are given for the measurements with the BSA-modified tip in comparison to unmodified tip; work of adhesion and surface free energy were obtained with the BSA-modified tip; change to the unmodified tip given in brackets. (Analysis of the significance was evaluated for all force curves with one-way ANOVA. For all formulations $p < 0.001$.) [b] Mass ratio at half-max were obtained by sigmoidal fitting of the data derived from densitometry (see Figure 3). As these values correspond to particle−protein ratios, a high value means low particle−protein interaction ($R^2 > 0.97$ for all particles tested). [c] Data were obtained by quantification and fitting of the BSA signal only from dispersion of the particles in complex FCS solution with AUC. [d] Obtained from mass-linear interference signal in AUC size distribution in FCS solution (see Figure 4). [e] n.d. = not determined.

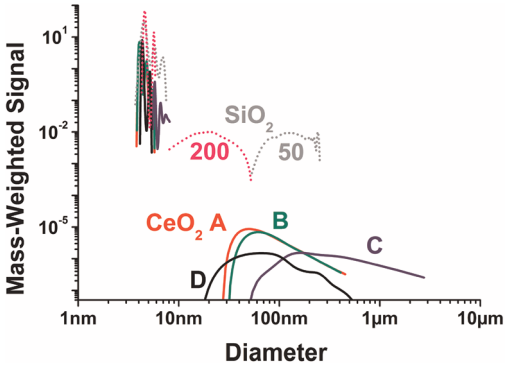

Figure 4. Size distribution of the SiO_2 particles (dotted lines) and CeO_2 particles (solid lines) after dispersion in FCS solution by AUC (particle−protein ratio of 1:1). The signal at 3−7 nm corresponds to the sizes of the BSA monomer and dimer, respectively. Clearly, the CeO_2, but not the SiO_2 particles deplete the free BSA.

State of Agglomeration with Analytical Ultracentrifugation. The interaction between colloids, and hence their tendency to agglomerate, may be reasonably assumed to be governed by their surface properties, including the spontaneous change of surface properties due to protein adsorption. We characterized the state of agglomeration in FCS by AUC with interference detection. Since the signal height is directly linear with the concentration in the measurement interval, the dispersed fraction (below 1 μm diameter) can be quantified (see Table 2). In Figure 4, the resulting particle size distributions are shown with logarithmic axes. SiO_2 50 and SiO_2 200 are very well dispersed in FCS solution, as the fraction <1 μm is 95 ± 5 wt %. For CeO_2 A and CeO_2 B in the presence of serum, around 25 wt % is dispersed for both, whereas CeO_2 C agglomerated more strongly with dispersibility below 10 wt %. Compared to CeO_2 A or B, CeO_2 C has 2 orders of magnitude fewer particles dispersed to 100 nm diameter or below. The smaller primary particle size of CeO_2 D is reflected in the small diameters also for its agglomerates, but the total dispersibility is as low as for CeO_2 C. The two-peaked signal below 10 nm diameter is attributed to the serum proteins. The peaks can be converted from diameters to molar masses, giving 65 and 120 kDa, in excellent agreement with BSA monomer and dimer. Again, the signal of the proteins is integrated and divided by the known protein refractive index increment dn/dc = 0.18 cm^3/g to provide an independent measurement of the actual concentration of the protein fraction that is not adsorbed on particles (see Table 2).

AFM Force−Distance Measurements between Proteins and Particles. Multiple preparations of adhesion force curves can be summarized as frequency distribution patterns (see Figure 5). Measuring adhesion with an unmodified AFM tip clearly reveals similar properties in a normal adhesion force distribution for all CeO_2 NPs (see Figure 5). The same experiments with covalently attached BSA at the apex of the tip reveals an increase of 24% (up to 3.9 nN) for CeO_2 A and of 12% (up to 3.6 nN) for CeO_2 B and lower interactions for CeO_2 C (−21%; down to 2.94 nN) and CeO_2 D (−37%; down to 3.32 nN).

The results of adhesion measurements of each CeO_2 formulation are summarized in Table 2. The calculated indention depths for CeO_2 A and CeO_2 B particles were lower after BSA modification. In contrast the indention depth of CeO_2 C and CeO_2 D increases.

The work of adhesion and surface free energy for the formulations using unmodified tips show an increasing order of the different particles. With unmodified tips CeO_2 D has the highest W_{adh} and CeO_2 A the lowest W_{adh}. BSA modification increased the W_{adh} for CeO_2 A and CeO_2 B; in contrast there is a major decrease for CeO_2 C and CeO_2 D particles.

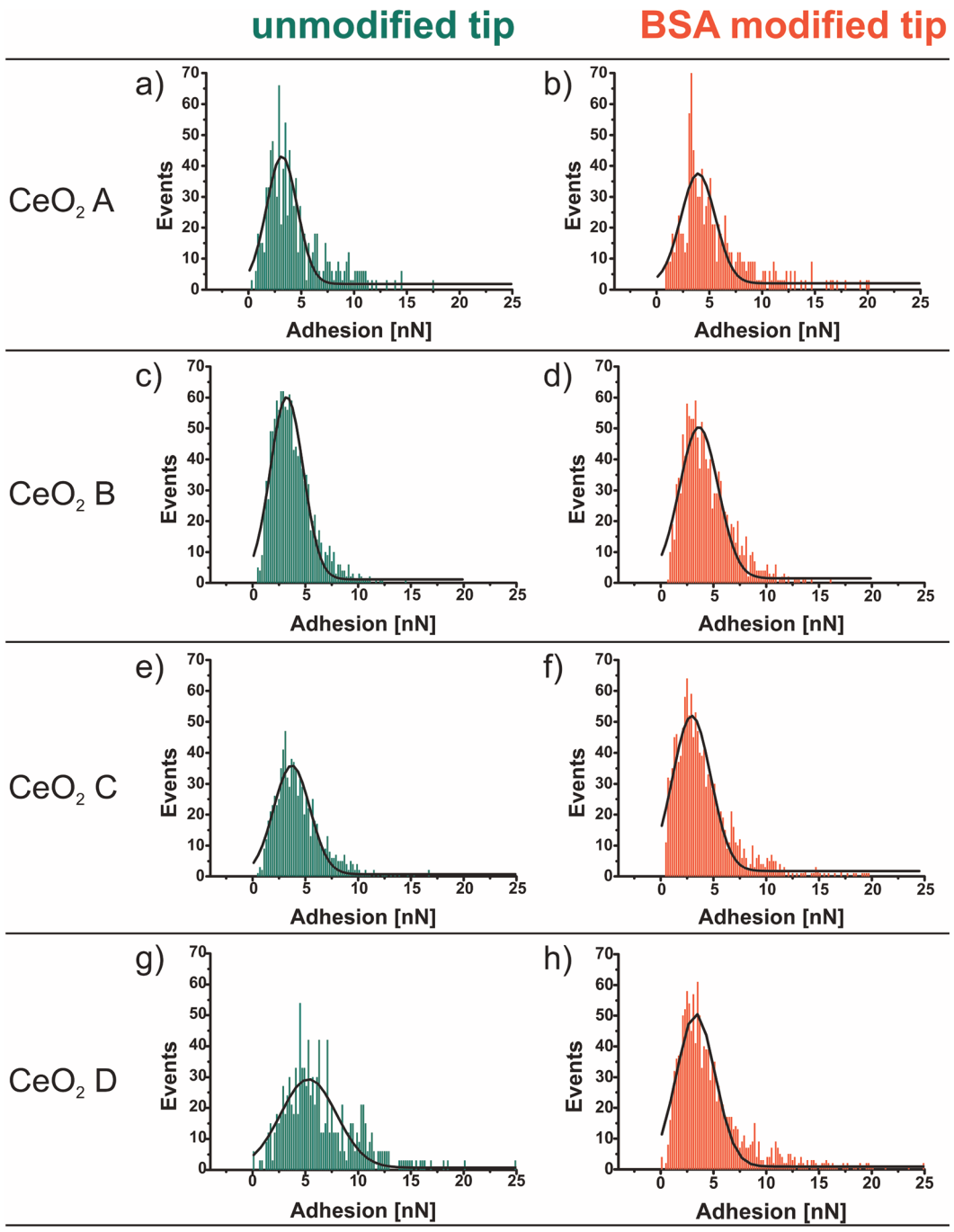

Figure 5. Frequency distribution of the adhesion values in the AFM force–distance curves: values obtained with (a) unmodified tip on CeO_2 A (n = 969), F_{adh} = 3.17 nN (w = 2.9); (b) BSA-modified tip on CeO_2 A (n = 972), F_{adh} = 3.93 nN (w = 3.2); (c) unmodified tip on CeO_2 B (n = 1251), F_{adh} = 3.23 nN (w = 3.1); (d) BSA-modified tip on CeO_2 B (n = 1240), F_{adh} =3.61 nN (w = 3.6); (e) unmodified tip on CeO_2 C (n = 832), F_{adh} = 3.71 nN (w = 3.4); (f) BSA-modified tip on CeO_2 C (n = 1283), F_{adh} = 2.94 nN (w = 3.6); (g) unmodified tip on CeO_2 D (n = 1071), F_{adh} = 5.30 nN (w = 5.3); and (h) BSA-modified tip on CeO_2 D particles (n = 1329), F_{adh} = 3.32 nN (w = 3.6). (The mode of F_{adh} was calculated from the Gauss fit of the curves.)

DISCUSSION

Generally, different particle characteristics are known to determine protein (*e.g.*, BSA) adsorption onto nanoparticles, and in particular hydrophobic interactions tend to be the dominating feature.[19−21] Also, electrostatic interactions can play a role,[22−25] and there is strong evidence that the size of the particle may be another factor influencing protein adsorption.[12,14] Clearly, not all proteins show the same adsorption patterns. Conditioning of different particles with complex protein mixtures, *e.g.*, blood serum, leads to different adsorption patterns for the protein fractions.[7,14,26,27] There are some mathematic models to fit protein adsorption data, which, however, require rather well-defined conditions: BSA adsorption onto chitosan-coated magnetic nanoparticles could be fitted to

Langmuir isotherms and hence quantified in terms of not only overall protein adsorption but also protein affinity.[23] The complexity of the subject is reflected by the work of Xia *et al.*: They used 28 marker molecules to predict the adsorption of small molecules such as testosterone.[4] This illustrates the need for new methods for the investigation of protein adsorption, as proteins are even much more complex. In this context, we interpret the protein adsorption data obtained with SiO_2 and CeO_2 nanoparticles.

There are several studies reporting protein adsorption onto SiO_2 nanoparticles: Walczyk and co-workers measured the protein corona after incubation in serum with differential centrifugal sedimentation and TEM.[9] Tenzer and colleagues even reported a complete proteomic approach of the particle corona of amorphous silica particles after incubation in serum.[14] In contrast to these reports, we could not find any protein adsorption above the detection limit for SiO_2 50 and 200 by neither SDS-PAGE nor AUC. The SiO_2 nanomaterials used in this study (Levasil 50 and 200, respectively) are stabilized by small amounts of alkaline, resulting in a negative charge of the nanoparticles and a slightly alkaline pH when dispersed in water (see Table 1). Neither lowering the pH of the aqueous particle dispersion to 6 nor dispersion in physiological phosphate buffered saline increased the BSA adsorption to detectable amounts (see Supporting Information, Figures S1−S3). Almost no binding of BSA to the surface of untreated silica nanoparticles was reported before by Rezwan *et al.*[28] even after 16 h of incubation at pH 7. The reason for the observed lack of protein binding in some of these studies remains to be further resolved. At this stage, we can only speculate that perhaps electrostatic repulsion between both the negatively charged protein and nanoparticle surface might be responsible. A phenomenological protein adsorption model taking into account the complex interfacial interactions at charged surfaces has recently been described by Hartvig *et al.*[29] The fact that proteins under competitive binding conditions bind differentially, based on affinities as well as there being protein concentration effects, adds additional complexity to this phenomenon.[8]

For CeO_2 particles, different nanoparticle−protein relations lead to different amounts of adsorbed protein: In spite of apparently similar physicochemical properties the protein interactions of the four CeO_2 nanoparticles show striking differences. Table 1 reveals that all four batches of CeO_2 particles are in a similar range regarding hydrodynamic diameter, zeta potential, and pH. XPS measurements revealed only minimal differences in surface chemistry for all particles tested. However, contact angle, time-of-flight secondary ion mass spectrometry (TOF-SIMS), and X-ray diffraction (XRD) revealed differences for CeO_2 D, as its surface energy was higher; the surface contained much fewer organic impurities and partially revealed an amorphous structure, which was confirmed by TEM pictures (see Figure 2). Those differences might be explained by the different preparation techniques for CeO_2 A to C (flame pyrolysis)[17] and CeO_2 D (precipitation).[18]

In general, AFM force measurements can be used to confirm high affinity to surfaces, which often corresponds to strong interactions between protein and the respective particle surface. As such measurements are always conducted under forced conditions (tip is pressed to the particle surface and the protein forced to interact with the surface), they are meaningful only if protein surface interactions also occur without additional forces. As no protein adsorption was found for the SiO_2 nanomaterials from aqueous solutions, we refrained from performing AFM force measurements with such particles.

Although the physicochemical properties of CeO_2 A to C are relatively similar, but different from those of CeO_2 D, the frequency distributions of the adhesion measurements showed differences among the four batches. The adhesion forces between a silicon tip with a 2−4 nm thick SiO layer and CeO_2 A NP increase by modifying the tip with BSA. Similar results with the AFM force measurements were obtained for CeO_2 B particles. For CeO_2 C and D the adhesion forces decrease after tip modification. This leads to the assumption that CeO_2 A and B have a higher affinity to BSA than to the unmodified AFM tip. Although CeO_2 C and D differ in some of their physicochemical properties, they show an inverse behavior: the affinity to the unmodified tip seems to be higher than to BSA.

It is known that proteins are flexible and that albumin changes its conformation on a surface in order to minimize interface energy. Gao *et al.* described a conformational changing of BSA molecules from α-helix to the more space requiring β-sheets.[30] These possible changes in the conformation of the structure of the adsorbed proteins can explain the different indention values of CeO_2 C and D: The indention increases for the BSA-modified tip for CeO_2 C compared to the indention with an unmodified cantilever, while all absolute indention values are lower than the BSA hydrodynamic diameter of 4.5 nm (data not shown). It seems that BSA adsorbs in a more stretched configuration on CeO_2 A and CeO_2 B, but stays more extended on CeO_2 C and D. This points to a lower affinity of BSA on CeO_2 C and D, which is in good correlation to the decrease in the adhesion forces.

Comparing these results with the data from the analytical ultracentrifugation, we obtain similar results. At a 1:1 ratio of nanoparticles and proteins, the agglomerate diameter distributions of CeO_2 A and CeO_2 B are identical except for an insignificant shift in diameter. The tendency to agglomerate is moderate, with more than 10 wt % of the particles dispersed below 100 nm diameter. We attribute this low level of

agglomeration to the presence of adsorbed proteins acting as protection colloids in steric stabilization. In contrast, CeO_2 C and CeO_2 D are characterized by a factor 2.5 lower dispersibility and vanishing fractions below 100 nm. Despite their significantly different primary particle size, both nanomaterials show a similar state of agglomeration, which we interpret to be a result of the lack or ineffectiveness of a stabilizing corona.

For BSA adsorption from BSA solution, all four nanomaterials showed adsorption isotherms with Hill slopes in a range of 0.5 to 1.8, detected by densitometry. This points to a noncooperative binding process; that is, already adsorbed protein does not facilitate further protein adsorption. As CeO_2 C and D revealed much smaller Hill slopes than CeO_2 A and B do, this is a further indicator for different adsorption behavior between the two groups, but high similarity among the groups.

Our data could not be fitted to Langmuir isotherms, but fitting to a sigmoidal model was successful, similarly as proposed previously by Röcker *et al*. for protein adsorption data derived from fluorescence correlation spectroscopy.[13] We believe this is due to the correlation between the level of agglomeration and the protein concentration: The particulate surface that is available for adsorption is not independent of the protein concentration, as proteins can improve dispersion of the particles, which leads to smaller particle sizes (deagglomeration) and hence to a larger surface available for protein adsorption.[31] In well-defined colloidal systems, such as stable polymer particle dispersions with uniform particle sizes, this effect does not occur. Also, our adsorption patterns are derived from a mixed influence of electrostatic and hydrophobic interactions (and maybe from different curvatures due to irregular particle shapes). Protein adsorption does not necessarily occur directly to the particle, but can also be mediated by other substances. Here, the adsorption of the 96% pure BSA seemed not to be mediated by impurities of the purchased protein but was a direct particle−protein interaction, as there was no significant difference in adsorption compared to highly pure BSA (data not shown). Also, the adsorption of proteins can be facilitated by already adsorbed proteins (cooperative binding) and can even be replaced by them later on.[8] The Hill slopes for the adsorption data of FCS (densitometry), being much larger than those for BSA in the case of all four nanomaterials, suggest such cooperative binding to occur for BSA when adsorbed from FCS solution. As albumin adsorbs on the surface of nanoparticles in a single layer,[13] one might speculate that the adsorption of other FCS proteins partially blocks the surface of the particles, leading to a faster, but overall lower mass of BSA adsorption.

CONCLUSION

Starting only with the intention to determine structure−effect relationships of nanomaterials by a variety of established physicochemical methods (*e.g.*, XRD, XPS, SIMS, BET surface, particle size, zeta potential), we must conclude that these are not sufficient to predict the adsorption of proteins and thus the resulting biological fate and effects of nanomaterials. For some industrially relevant SiO_2 nanomaterials no protein binding could be quantified within the detection limit, while for the CeO_2 nanomaterials protein binding was very prominent. For all four batches of the same material (CeO_2), showing at most minimal differences in their physicochemical surface characteristics, considerable variations in the adsorption of serum proteins (using albumin as marker) were nevertheless observed. These differences in protein binding could not be explained by the intrinsic physicochemical material characteristics alone. As we could show, among the various contemporary biophysical methods in particular AFM, AUC, and SDS-PAGE in combination with densitometry are powerful tools to characterize protein adsorption to nanomaterials. To understand and predict the biological properties of nanomaterials, the implementation of these techniques appears highly advisible. As it is known that very likely this protein corona is "what the cell sees" and defines its further processing in the human body, such *in situ* or *as-tested* characterization, and not only *as-produced*, is required for a reliable safety assessment.

MATERIALS AND METHODS

Materials. Phenyltrimethoxysilane (Dynasylan 9165) and (3-aminopropyl)triethoxysilane (Dynasylan AMEO) were a gift from Degussa GmbH, Düsseldorf, Germany. *N*,*N*-Diisopropylethylamine and cyanuric chloride were purchased from Sigma-Aldrich Chemie GmbH, Munich, Germany. Trichloromethane and methanol were purchased from Carl Roth GmbH + Co. KG, Karlsruhe, Germany. Water was either purified by reverse osmosis (Millipore Synthesis, Schwalbach/Ts., Germany) or double distilled prior to use. AFM tips CSC 37/noAl were purchased from Micromasch, Estonia. The bovine serum albumin and all chemicals for SDS-PAGE were purchased from Sigma Aldrich, Germany. Fetal bovine serum Gold came from PAA, Germany. CeO_2 D was kindly provided by G. Gregori.[18] Fermentas PageBlue Coomassie staining reagent was purchased from Thermo Scientific, Germany.

Physicochemical Characterization of Particles. The hydrodynamic diameters of metal oxide nanoparticles were determined by DLS using a Zetasizer Nano ZS from Malvern Instruments (Herrenberg, Germany) equipped with a 10 mW HeNe laser at a wavelength of 633 nm at 25 °C, essentially as described previously.[32] Scattered light was detected at a 173° angle with laser attenuation and measurement position adjusted automatically by the Malvern software. Values given are the means ± standard deviation of three independent experiments with each experiment including three measurements of the same sample with at least 10 runs each, as determined by the Zetasizer.

The zeta potential of the nanoparticles was determined by laser Doppler electrophoresis using a folded capillary electrophoresis cell of the Zetasizer Nano ZS at 25 °C, with the light signal detected at a 17° angle. Nanoparticles were dispersed in double-distilled water with a concentration of 10 mg/mL and incubated for 30 min in an ultrasonic water bath at room temperature. The average value was calculated with the data of three times 10 runs ± standard deviation.

TEM Imaging. A carbon-coated 300 mesh TEM grid was dipped into a dispersion with a concentration of 0.1 mg/mL in 2-propanol for CeO_2 and 0.1 mg/mL in water for SiO_2, respectivley. The crystal structure and crystalline appearance were visualized using TEM imaging on a Jeol JEM-3010 TEM (Jeol Ltd., Tokyo, Japan) with 300.000 V.

XRD Crystallinity Measurement. Crystallinity was determined by X-ray diffraction. The intensity of the diffracted X-ray beam was recorded by a D8 Advance (Fa. Bruker/AXS) as function of the diffraction angle ($2° < 2\theta < 150°$). Quantitative phase analysis was performed using Rietveld refinement.

XPS Detection of Particle Impurities and Surface Modifications. Impurities and surface modification was determined by X-ray photoelectron spectroscopy with a Phi XPS 5500 system with 300 W monochromatic Al Kα radiation, a pass energy for surveys of 117 eV (measurement time of 45 min), and detailed spectra at 23.5 eV (measurement time of 6 min). Evaluation was performed by CasaXPS 2.3.15, based on phi standard-sensitivity factors, with Shirley background subtraction and peak shape fits as a sum of 90% Gaussian and 10% Lorentzian. Information depth is limited to the surface 10 nm of the material. We performed two measurements per sample, each integrating over 0.5 mm^2. The results in percentage are derived from the relative concentration of elements and their chemical bonds from line shape analyses.

TOF-SIMS Characterization of Particles. Static TOF-SIMS spectra were recorded using a TOF-SIMS V spectrometer (Iontof GmbH, Germany). A pulsed mass-filtered primary ion beam of 25 keV singly charged bismuth (Bi^+) was used. This primary ion beam, resulting in a spot size of typically 5 μm on the sample surface, was raster scanned over an area of 250 × 250 μm to record spectra of positive and negative secondary ions. The rastered area integrates over more than 10^6 particles. The primary ion dose density was always kept well below 10−12 ions cm^{-2} and thus in the static SIMS regime. To prevent charging of the sample surface, a low-electron energy flood gun was used. The sample particle sediments were prepared for SIMS analysis by placing them on clean silicon wafers. On the thus prepared sample positions, no silicon wafer secondary ion mass signal could be detected any more, confirming that the sample layer thickness well exceeded the SIMS information depth of typically 1−3 nm.

Contact Angle Measurements for CeO_2 A to D. A thin planarized nanoparticle film of 1 mm thickness was immobilized with a 100 μm thick glue film on a PTFE foil. After removing the nonimmobilized powder the sample was treated with filtered nitrogen. The contact angles were measured with drops of water, formamide, and diiodomethane. The drops were imaged onto a CCD, and contact angles were extracted by standardized software.

Inverse Gas Chromatography for the SiO_2 50 and 200 and CeO_2 B and C Particles. Inverse gas chromatography[33] is based on the study of interactions of gas molecules of known properties with a solid surface. Small amounts of molecular probes are injected into the stream of the carrier gas flowing through the chromatographic column filled with the solid to be investigated (Surface Energy Analyzer, SMS, Alpteron, UK). The columns were packed with 8 to 50 mg of nanomaterial and conditioned for 1 h at 60 °C and 20 sccm helium flux. The unpolar (nonane, octane, heptane) and polar (dichloromethane, acetonitrile, acetone, ethylacetate) test gases were injected at 30 °C, and the retention time was analyzed to give the interaction energies.

AFM Measurements: Tip Calibration. AFM tips (CSC 37/noAl, Micromasch, Estonia) were mounted on an atomic force microscope (Nanowizard, JPK Instruments, Berlin, Germany). A force spectroscopy experiment was performed on purified glass to determine the sensitivity of the setup. For this, glass was presumed to be not indentable. The spring constants of the AFM tips were determined using the built-in algorithm, which relies on a method described by Hutter *et al.*[34]

AFM Measurements: Tip Modification. To remove production residues and contaminations, AFM tips were precleaned as described by Hinterdorfer *et al.*[35] Briefly, they were consecutively incubated in peroxymonosulfuric acid and trichloromethane and dried in a dry air flow. Besides the cleaning effect, this method results in an enrichment of free silanol groups at the surface of the AFM tip. These silanol groups were used to facilitate silanization. First, a layer of Dynasylan 9165 was attached to the AFM tip by incubation in an organic solution of the silane (20 μL/mL trichloromethane) for 30 min. Subsequently, the AFM tips were washed by dipping them into trichloromethane, methanol, and water, consecutively. After this, the apex of the AFM tip was silanized with Dynasylan AMEO by 30 min incubation of the tips in an organic solution of the silane (20 μL/mL trichloromethane). This was followed by washing the tips in trichloromethane, methanol, and water, consecutively. AFM tips were heated to 105 °C for 1 h in a cabinet heater. Subsequently, the AFM tips were incubated in a solution of cyanuric chloride (1 mg/mL trichloromethane) containing 10 μL of *N*,*N*-diisopropylethylamine for 2 h and washed by dipping them into trichloromethane and water. To attach BSA to the AFM tips, the pretreated tips were incubated in an aqueous BSA solution (10 mg/mL) for 12 h and afterward washed with water.

As aromatic silane layers have been reported to be hydrophilic enough not to show repulsion when approached to a surface,[36] Dynasylan 9165 was used to inactivate the side faces of the AFM tip. After removing the inactive faces a layer of Dynasylan AMEO was applied to the cleaned apex, facilitating covalent coupling of the protein to the AFM tip.

Particle−Protein Interaction by Atomic Force Microscopy. In an atomic force microscopy experiment, forces are determined as deflection (d) of the cantilever. With the spring constant (k_c) of the cantilever given, this applied force (F_{adh}) can be calculated from the detected deflection by Hooke's law (eq 1).[37] For this, the exact determination of the spring constant and sensitivity of the cantilever, to which the AFM tip is mounted, are crucial prerequisites for reliable force spectroscopy experiments. For both, there is a proportional relation to the value of the force measured in an experiment.[38] First, the sensitivity of the setup was determined three times. To determine the spring constant, the mean value of these experiments was used. Spring constants were determined three times for each tip and were all within the range of the manufacturer's specifications (SD < 10%). Prior to each experiment, the AFM sensitivity was determined again, because every change in the setup (*e.g.*, position of the laser on the backside of the cantilever) may change the sensitivity.

$$F_{adh} = k_c d \quad (1)$$

F_{adh} = force; k_c = spring constant; d = deflection.

For each experiment a drop of the particle dispersion, pretreated in a bath sonicator for 3 min, was dried onto a glass slide, resulting in a thin homogeneous film of the particles. Films were visualized in intermittent contact (air) mode.

In each experiment 64 adhesion measurements were performed on an area of 4 μm^2 with 0.5 μm z-length and a retraction time of about 0.5 s. The experiments were done 10 times with three individual tips, each for unmodified and BSA-modified tips, to optimize the measurement setup regarding tip curvature, spring constant, *etc.* After each experiment the tip was checked for dramatic changes.

From these adhesion measurements the work of adhesion (W_{adh}) was calculated according to James *et al.*[39] using the formula

$$W_A = \frac{3F_{adh}}{2\pi R} \quad (2)$$

F_{adh} = force; R = tip radius.

According to the JKR (Johnson, Kendall, Roberts) theory, R is the radius of the hemispherical point of contact. After each

experiment the tip appearance was checked for dramatic changes. Using eq 3 the surface free energy (γ_1) was calculated subsequently. According to James *et al.* and Davies *et al.*,[39,40] the surface free energy of the silicon tip is determined using the contact angle technique range from approximately 41 to 43 mJ m^{-2}. In this study the value of the surface free energy of the silicon tips (γ_2) was fixed to 42 mJ m^{-2}. The indention of the particle deformation was calculated from the differences in the slope of the force−distance approach curve between glass as reference and the sample surface.

$$\gamma_1 = \frac{W_{adh}{}^2}{4\gamma_2} \quad (3)$$

W_{adh} = work of adhesion; γ_2 = surface free energy of tip.

Agglomeration Control by Analytical Ultracentrifugation. The particle size distribution was determined by an AUC of ~500 μL of the test dispersion with a mass ratio of nanomaterial:FCS proteins = 2:1.

Simultaneous detection by synchronized interference optics (Beckmann, model XLI) quantified the amount and the diameter of each fraction independently from 1 nm up to several micrometers diameter.[41,42] We can thus successively quantify in a single measurement the protein content, the protein molar mass, the nanomaterial content, and the nanomaterial state of agglomeration. When the retrieved concentration of proteins is less than 100 wt % at the expected molar mass, we assume that the remaining proteins have adsorbed to a particulate surface. When the retrieved concentration of nanomaterial is less than 100 wt % in the measurement interval, we assume that the remainder has agglomerated beyond 1 μm diameter. The evaluation of the AUC raw data incorporated the loose packing of nanoparticle agglomerates by assigning to them a fractional dimension and using the fractal agglomerate sedimentation relation as specified in eq 6 of ref 43. We used a value of 2.1 for the fractional dimension, which is universal for the morphology of agglomerates from reaction-limited colloidal association (*i.e.*, reversible agglomeration).[43,44] A fractional dimension of 3 describes solid spheres and is employed, for example, in routine DLS or photon correlation spectroscopy evaluation, but is obviously wrong for agglomerates. The tabulated material's constant of refractive index allows the interference optics to linearly directly quantify the fraction that is dispersed to diameters below 100 nm in the actual test preparation, with the full size distributions. The value for the nanodispersed fraction is regarded as an upper limit, judging from the comparison of size determination methods with different physical measurement principles.[31]

Indirect Determination of Protein Adsorption to Nanoparticles. Nanoparticles were predispersed for 1 h in dispersion medium prior to mixture with the same volume of protein solution, leading to particle−protein ratios from 1:10 up to 100:1. For the explicit dispersion media and particle and protein concentrations for BSA and FCS, see Tables 3 and 4. No differences were found concerning the protein denaturation or precipitation caused by dilution of FCS in water or PBS, respectively (tested with SEC, see Supporting Information). The resulting dispersions were stirred at room temperature for 1 h at 300 rpm, transferred into Eppendorf tubes, and centrifuged at 23000*g* for 45 min and 10 °C in a Hettich Universal 30 RF with E1175 rotor. Afterward, the supernatants were collected and the pellets washed once with deionized water. The pellets were resuspended directly in 2× sample buffer, and supernatants were diluted as described in Tables 3 and 4 and also mixed with the same volume of sample buffer. Afterward SDS-PAGE was performed as described elsewhere.[45] The gels were stained with Coomassie dying solution following the manual and scanned with the computer program Image Lab V 4.0 (BioRad, Munich, Germany). BSA bands of the supernatants were read out and compared to the band of the corresponding negative control. As especially at the high particle−protein ratios the proteins could not be detached from the CeO_2 particles anymore, there was not always a protein band for all sample pellets, as the adsorbed proteins could not be detached from the particles and did not migrate into the gel (see Supporting Information, Figures S4 and S5). Hence, the protein bands of the different supernatants had to be compared and subtracted from the total protein signal to determine the adsorbed amount of protein indirectly.

TABLE 3. Experimental Setup for the Determination of Protein Adsorption from BSA Solution

nanoparticles	dispersion media	protein end concentrations of BSA [mg/mL]	dilution of supernatants for SDS-PAGE after centrifugation
SiO_2 50 and 200	water/water,	100	1:1000
[10 mg/mL]	adjusted to	10	1:100
	pH 6/PBS	2	1:20
		1	1:10
		0.1	no dilution
CeO_2 A−D	water	100	1:1000
[10 mg/mL]		10	1:100
		2	1:20
		1	1:10
		0.1	no dilution

TABLE 4. Experimental Setup for the Determination of Protein Adsorption of BSA from FCS Solution

nanoparticles	dispersion media	protein end concentrations of BSA [mg/mL]	dilution of supernatants for SDS-PAGE after centrifugation
SiO_2 50 and	water	19	1:1000
200 [1.9 mg/mL]/CeO_2		1.9	1:100
A−D [1.9 mg/mL]		0.38	1:20
		0.19	1:10
		0.019	no dilution

Sigmoidal Fitting and Determination of Half-Maximum Values from the Adsorption Data. The protein adsorption data from densitometry were plotted against the different particle−protein ratios (w/w) used and fitted with a heuristic sigmoidal model with the equation

$$y = A_1 + \frac{A_2 - A_1}{1 + 10^{((\log(x_0 - x))}} \quad (4)$$

where A_1 is the initial value, A_2 the maximum of adsorption, and x_0 the mass ratio at half-maximum adsorption. As the adsorption tends to 100% with increasing particle−protein ratio, A_2 was set and fixed at a value of 100% and A_1 at a value of 0%; the Hill slope p, which corresponds to the steepness of the curve, was kept variable. For the fits containing a 20-point set between A_1 and A_2, left and right margins were set to 0, and 20 fit iterations were performed. From these sigmoidal fits, half-maximum values were read out. All calculations were performed with the computer program Origin 6.0 (Microcal).

Conflict of Interest: The authors declare no competing financial interest.

Acknowledgment. We thank Mr. R. Fritz of the working group of Mrs. K. Volz (Marburg) for the TEM images, Mr. R. Stark for discussions on AFM interpretation, and Mr. B. von Vacano (BASF SE) for SIMS and surface characterization. J.S., E.E.J.M., and U.B. thank the DFG for financial support (DFG FOR 627 "Nanohale"). We thank Mr. G. Gregori and Mr. M. Göbel (MPI, Stuttgart) for kindly providing pure CeO_2. Also, we thank the Federal Ministry of Education and Research BMBF (Project "NanoCare", Förderkennzeichen 03X0021C) for financial funding.

Rene Rietscher is thanked for the SEC analysis, and Julian Kirch for his input to the discussion.

Supporting Information Available: Characterization of SiO_2 nanoparticles in different dispersion media, size exclusion chromatography, as well as SDS-PAGE results of protein adsorption on CeO_2 and SiO_2 nanoparticles. This material is available free of charge *via* the Internet at http://pubs.acs.org.

REFERENCES AND NOTES

1. Lynch, I.; Salvati, A.; Dawson, K. A. Protein-Nanoparticle Interactions: What Does the Cell See? *Nat. Nanotechnol.* **2009**, *4*, 546–547.
2. Van Hoecke, K.; Quick, J.; Mankiewicz-Boczek, J.; De Schamphelaere, K.; Elsaesser, A.; Van der Meeren, P.; Barnes, C.; McKerr, G.; Howard, C.; Van der Meent, D.; *et al*. Fate and Effects of CeO_2 Nanoparticles in Aquatic Ecotoxicity Tests. *Environ. Sci. Technol.* **2009**, *43*, 4537–4546.
3. SCENIHR. *Risk Assessment of Products of Nanotechnologies*; SCENIHR, Ed.; January 19, **2009**.
4. Xia, X. R.; Monteiro-Riviere, N. A.; Riviere, J. E. An Index for Characterization of Nanomaterials in Biological Systems. *Nat. Nanotechnol.* **2010**, *5*, 671–675.
5. Lindman, S.; Lynch, I.; Thulin, E.; Nilsson, H.; Dawson, K. A.; Linse, S. Systematic Investigation of the Thermodynamics of HSA Adsorption to *N-iso*-Propylacrylamide/*N-tert*-Butylacrylamide Copolymer Nanoparticles. Effects of Particle Size and Hydrophobicity. *Nano Lett.* **2007**, *7*, 914–920.
6. Lundqvist, M.; Stigler, J.; Elia, G.; Lynch, I.; Cedervall, T.; Dawson, K. A. Nanoparticle Size and Surface Properties Determine the Protein Corona with Possible Implications for Biological Impacts. *Proc. Natl. Acad. Sci. U. S. A.* **2008**, *105*, 14265–14270.
7. Monopoli, M. P.; Bombelli, F. B.; Dawson, K. A. Nanobiotechnology: Nanoparticle Coronas Take Shape. *Nat. Nanotechnol.* **2011**, *6*, 11–12.
8. Monopoli, M. P.; Walczyk, D.; Campbell, A.; Elia, G.; Lynch, I.; Bombelli, F. B.; Dawson, K. A. Physical-Chemical Aspects of Protein Corona: Relevance to *in Vitro* and *in Vivo* Biological Impacts of Nanoparticles. *J. Am. Chem. Soc.* **2011**, *133*, 2525–2534.
9. Walczyk, D.; Bombelli, F. B.; Monopoli, M. P.; Lynch, I.; Dawson, K. A. What the Cell "Sees" in Bionanoscience. *J. Am. Chem. Soc.* **2010**, *132*, 5761–5768.
10. Landsiedel, R.; Ma-Hock, L.; Kroll, A.; Schnekenburger, J.; Wiench, K.; Wohlleben, W. Testing Metal-Oxide Nanomaterials for Human Safety. *Adv. Mater.* **2010**, *22*, 2601–2627.
11. Yang, K.; Lin, D.; Xing, B. Interactions of Humic Acid with Nanosized Inorganic Oxides. *Langmuir* **2009**, *25*, 3571–3576.
12. Cedervall, T.; Lynch, I.; Lindman, S.; Berggård, T.; Thulin, E.; Nilsson, H.; Dawson, K. A.; Linse, S. Understanding the Nanoparticle-Protein Corona Using Methods to Quantify Exchange Rates and Affinities of Proteins for Nanoparticles. *Proc. Natl. Acad. Sci. U. S. A.* **2007**, *104*, 2050–2055.
13. Rocker, C.; Potzl, M.; Zhang, F.; Parak, W. J.; Nienhaus, G. U. A Quantitative Fluorescence Study of Protein Monolayer Formation on Colloidal Nanoparticles. *Nat. Nanotechnol.* **2009**, *4*, 577–580.
14. Tenzer, S.; Docter, D.; Rosfa, S.; Wlodarski, A.; Kuharev, J.; Rekik, A.; Knauer, S. K.; Bantz, C.; Nawroth, T.; Bier, C.; *et al*. Nanoparticle Size is a Critical Physicochemical Determinant of the Human Blood Plasma Corona: A Comprehensive Quantitative Proteomic Analysis. *ACS Nano* **2011**, *5*, 7155–7167.
15. Palmisano, P.; Faraldi, P.; Fino, D.; Russo, N. Household Oven Self-Cleaning Surfaces via Catalytic Thermal Oxidation. *Chem. Eng. J.* **2009**, *154*, 251–257.
16. Jung, H.; Kittelson, D. B.; Zachariah, M. R. The Influence of a Cerium Additive on Ultrafine Diesel Particle Emissions and Kinetics of Oxidation. *Combust. Flame* **2005**, *142*, 276–288.
17. Kuhlbusch, T. A. J.; Krug, H. F.; Nau, K. *NanoCare, Health Related Aspects of Nanomaterials, Final Scientific Report*, 1st ed.; DECHEMA e.V.: Frankfurt a.M., **2009**.
18. Gobel, M. C.; Gregori, G.; Guo, X.; Maier, J. Boundary Effects on the Electrical Conductivity of Pure and Doped Cerium Oxide Thin Films. *Phys. Chem. Chem. Phys.* **2010**, *12*, 14351–14361.
19. Gessner, A.; Waicz, R.; Lieske, A.; Paulke, B.; Mader, K.; Muller, R. H. Nanoparticles with Decreasing Surface Hydrophobicities: Influence on Plasma Protein Adsorption. *Int. J. Pharm.* **2000**, *196*, 245–249.
20. Israelachvili, J. N.; Pashley, R. M. Measurement of the Hydrophobic Interaction between Two Hydrophobic Surfaces in Aqueous Electrolyte Solutions. *J. Colloid Interface Sci.* **1984**, *98*, 500–514.
21. Luck, M.; Paulke, B. R.; Schroder, W.; Blunk, T.; Muller, R. H. Analysis of Plasma Protein Adsorption on Polymeric Nanoparticles with Different Surface Characteristics. *J. Biomed. Mater. Res.* **1998**, *39*, 478–485.
22. Koutsoukos, P. G.; Mumme-Young, C. A.; Norde, W.; Lyklema, J. Effect of the Nature of the Substrate on the Adsorption of Human Plasma Albumin. *Colloids Surf.* **1982**, *5*, 93–104.
23. Liang, Y.-Y.; Zhang, L.-M.; Li, W.; Chen, R.-F. Polysaccharide-Modified Iron Oxide Nanoparticles as an Effective Magnetic Affinity Adsorbent for Bovine Serum Albumin. *Colloid Polym. Sci.* **2007**, *285*, 1193–1199.
24. Shamim, N.; Hong, L.; Hidajat, K.; Uddin, M. S. Thermosensitive-Polymer-Coated Magnetic Nanoparticles: Adsorption and Desorption of Bovine Serum Albumin. *J. Colloid Interface Sci.* **2006**, *304*, 1–8.
25. Yoon, J.-Y.; Kim, J.-H.; Kim, W.-S. The Relationship of Interaction Forces in the Protein Adsorption onto Polymeric Microspheres. *Colloids Surf., A* **1999**, *153*, 413–419.
26. Cedervall, T.; Lynch, I.; Foy, M.; Berggard, T.; Donnelly, S. C.; Cagney, G.; Linse, S.; Dawson, K. A. Detailed Identification of Plasma Proteins Adsorbed on Copolymer Nanoparticles. *Angew. Chem., Int. Ed.* **2007**, *46*, 5754–5756.
27. Ehrenberg, M. S.; Friedman, A. E.; Finkelstein, J. N.; Oberdorster, G.; McGrath, J. L. The Influence of Protein Adsorption on Nanoparticle Association with Cultured Endothelial Cells. *Biomaterials* **2009**, *30*, 603–610.
28. Rezwan, K.; Meier, L. P.; Gauckler, L. J. Lysozyme and Bovine Serum Albumin Adsorption on Uncoated Silica and AlOOH-Coated Silica Particles: The Influence of Positively and Negatively Charged Oxide Surface Coatings. *Biomaterials* **2005**, *26*, 4351–4357.
29. Hartvig, R. A.; van de Weert, M.; Ostergaard, J.; Jorgensen, L.; Jensen, H. Protein Adsorption at Charged Surfaces: The Role of Electrostatic Interactions and Interfacial Charge Regulation. *Langmuir* **2011**, *27*, 2634–2643.
30. Gao, H.; Geng, X. P.; Wang, B. H.; Zhou, Y. Studies on the Conformational Change of Adsorbed BSA onto a Moderately Hydrophobic Surface at Different Denaturant Concentrations and Surface Coverages. *J. Colloid Interface Sci.* **2010**, *344*, 468–474.
31. Schulze, C.; Kroll, A.; Lehr, C.-M.; Schaefer, U. F.; Becker, K.; Schnekenburger, J.; Schulze Isfort, C.; Landsiedel, R.; Wohlleben, W. Not Ready to Use - Overcoming Pitfalls When Dispersing Nanoparticles in Physiological Media. *Nanotoxicology* **2008**, *2*, 51–61.
32. Höbel, S.; Prinz, R.; Malek, A.; Urban-Klein, B.; Sitterberg, J.; Bakowsky, U.; Czubayko, F.; Aigner, A. Polyethylenimine PEI F25-LMW Allows Long-Term Storage of Frozen Complexes as Fully Active Reagents in si-RNA-Mediated Gene Targeting and DNA Delivery. *Eur. J. Pharm. Biopharm.* **2008**, *70*, 29–41.
33. Voelkel, A.; Strzemiecka, B.; Adamska, K.; Milczewska, K. Inverse Gas Chromatography as a Source of Physiochemical Data. *J. Chromatogr., A* **2009**, *1216*, 1551–1566.
34. Hutter, J. L.; Bechhoefer, J. Calibration of Atomic-Force Microscope Tips. *Rev. Sci. Instrum.* **1993**, *64*, 1868.
35. Hinterdorfer, P.; Baumgartner, W.; Gruber, H. J.; Schilcher, K.; Schindler, H. Detection and Localization of Individual Antibody-Antigen Recognition Events by Atomic Force Microscopy. *Proc. Natl. Acad. Sci. U. S. A.* **1996**, *93*, 3477–3481.
36. Vakarelski, I.; Higashitani, K. Single-Nanoparticle-Mediated Tips for Scanning Probe Microscopy. *Langmuir* **2006**, *22*, 2931–2934.

37. Butt, H.-H.; Cappella, B.; Kappl, M. Force Measurements with the Atomic Force Microscope: Technique, Interpretation and Applications. *Surf. Sci. Rep.* **2005**, *59*, 1–152.
38. Leite, F. L.; Herrmann, P. S. P. Application of Atomic Force Spectroscopy (AFS) to Studies of Adhesion Phenomena: A Review. *J. Adhes. Sci. Technol.* **2005**, *19*, 365–405.
39. James, J.; Crean, B.; Davies, M.; Toon, R.; Jinks, P.; Roberts, C. J. The Surface Characterisation and Comparison of Two Potential Sub-Micron, Sugar Bulking Excipients for Use in Low-Dose, Suspension Formulations in Metered Dose Inhalers. *Int. J. Pharm.* **2008**, *361*, 209–221.
40. Davies, M.; Brindley, A.; Chen, X.; Marlow, M.; Doughty, S. W.; Shrubb, I.; Roberts, C. J. Characterization of Drug Particle Surface Energetics and Young's Modulus by Atomic Force Microscopy and Inverse Gas Chromatography. *Pharm. Res.* **2005**, *22*, 1158–1166.
41. Machtle, W.; Borger, L. *Analytical Ultracentrifugation of Polymers and Nanoparticles*; Springer: Berlin, 2006.
42. Planken, K. L.; Colfen, H. Analytical Ultracentrifugation of Colloids. *Nanoscale* **2010**, *2*, 1849–1869.
43. Lin, M. Y.; Lindsay, H. M.; Weitz, D. A.; Ball, R. C.; Klein, R.; Meakin, P. Universal Reaction-Limited Colloid Aggregation. *Phys. Rev. A: At., Mol., Opt. Phys.* **1990**, *41*, 2005–2020.
44. Evans, D. F.; Wennerström, H. *The Colloidal Domain: Where Physics, Chemistry, Biology, and Technology Meet*, 2nd ed.; Wiley-VCH: New York, 1999.
45. Schulze, C.; Schaefer, U. F.; Ruge, C. A.; Wohlleben, W.; Lehr, C.-M. Interaction of Metal Oxide Nanoparticles with Lung Surfactant Protein A. *Eur. J. Pharm. Biopharm.* **2011**, *77*, 376–383.